Approved, DCN# 43-10561-22

Characterization of Nitridated Ga_2O_3 for GaN-on-Ga_2O_3 Power Device Applications

Matthew M. Landi[1], Frank P. Kelly[1], Riley E. Vesto[1], Marko J. Tadjer[2], Karl D. Hobart[2], Kyekyoon Kim[1]

[1]*Department of Electrical and Computer Engineering, University of Illinois at Urbana-Champaign, Urbana, IL 61801, USA*
[2]*United States Naval Research Laboratory, Washington D.C., 20375, USA*
e-mail: kevinkim@illinois.edu, Phone: +1-(217)-333-7162

Keywords: Ga_2O_3, GaN, Nitridation, Characterization, PAMBE

Abstract

High-quality GaN growth on Ga_2O_3 necessitates a low defect density, therefore, careful engineering of the transition between substrate and epilayer is crucial to arrest defect propagation and reduce dopant compensation via intrinsic defects. A plasma-assisted molecular beam epitaxy (PAMBE) chamber equipped with a radio-frequency (RF) nitrogen source was used to nitridate β-Ga_2O_3 (-201) to wurtzite GaN (0001). The nitridated layers were characterized by X-ray diffraction (XRD), X-ray reflectivity (XRR), reflection high energy electron diffraction (RHEED), and atomic-force microscopy (AFM). Understanding the fundamental mechanisms governing the nitridation of Ga_2O_3 was facilitated through analysis of these characteristics, culminating in high-quality growth of unintentionally doped (UID) GaN on Ga_2O_3 by means of a nitridated GaN buffer layer.

INTRODUCTION

Next generation power device systems are looking to ultra-wide bandgap materials such as diamond, aluminum nitride (AlN), and β-Ga_2O_3 due to their high critical electric field strength, low on-resistance, and favorable carrier mobility properties which stand to improve performance of power systems beyond that of SiC and GaN [1,2]. Notably, β-Ga_2O_3 surpasses both GaN and SiC on Baliga's and Baliga's high-frequency figure of merit, and has low-cost, robust methods of substrate fabrication including floating zone, Czochralski, and edge-defined film fed growth which is widely implemented for sapphire wafer production [1]. Unfortunately, β-Ga_2O_3 is limited by low thermal conductivity and lack of *p*-doping, making it a challenge to design industry-ready devices which can achieve the theoretical 8 $MVcm^{-1}$ critical field strength [1-4]. One potential solution is to form a heterojunction to β-Ga_2O_3 with another wide or ultrawide bandgap material which compensates these weaknesses [1,5,6,10]. GaN is a promising candidate as β-Ga_2O_3 can be nitridated to its wide-bandgap nitride [10]; furthermore, GaN has mature processing and device fabrication documentation, including *p*-type activation [11,12]. Hetero-epitaxial processes employ buffer layers to reduce lattice strain and arrest defect propagation from the substrate. In the case of GaN-on-Ga_2O_3, both nitridated and epitaxial thin films have been attempted as buffer layers to varying degrees of success [5,6,10]. GaN and AlN epitaxy using MOCVD and MOVPE was successful in enhancing defect-arresting behavior at the interface as evidenced by moderate full width at half maximum (FWHM) of the (0002) reflection on the order of 330-450arcsec; however, improvements are still necessary before the crystalline quality is sufficient for *p*-type GaN epilayers [5,6]. Epitaxy of *p*-GaN requires low background *n*-type carrier density as to not immediately compensate the activated donors. Film characterization using X-ray diffraction (XRD) to assess the broadening of the (0002) reflection, commonly attributed to threading dislocation density, is therefore used to benchmark the performance of buffer layer techniques, deposition methods, and starting substrates; a lower FWHM indicates a reduced defect density. Furthermore, threading dislocations are known leakage centers in GaN devices and contribute to localized heating and poor device longevity due to their mobility under high electric field [9,12,13]. Therefore, it is crucial to understand the effect of nitridation conditions on their formation and propagation. Nitridated β- and ε-Ga_2O_3 have been reported, however, poor understanding of nitridation mechanisms, sources of lattice strain, and defect propagation leaves much to be discussed [7,10]. Moreover, a comprehensive mapping of nitridation conditions in PAMBE and their resulting impact have yet to be performed. In response, a nitridation process is developed through the systematic study of nitridation conditions in PAMBE, which include nitridation temperature and plasma power density. The nitridated surfaces were characterized via X-ray reflectivity (XRR), XRD, reflection high-energy electron diffraction (RHEED), and atomic force microscopy (AFM).

RESULTS AND DISCUSSION

Substrates of (-201) β-Ga_2O_3 were nitridated at temperatures ranging 600–725˚C, and nitrogen RF plasma source conditions ranging from 300-400W and 0.85–2.2sccm. This specific range was selected to probe GaN quality and nitridation mechanisms near the temperature threshold of GaN decomposition, reported in the range of 700˚C [8]. Phase evolution at the surface was monitored *in-situ* via RHEED. Figure 1 highlights the transformation from monoclinic Ga_2O_3 to wurtzite GaN at 700 ˚C under 400W 1.3sccm plasma conditions, corresponding to a flux of ~ 0.3 MLs^{-1}. Prolonged

DISTRIBUTION STATEMENT A. Approved for public release; distribution unlimited.

nitridation time resulted in surface roughening, as seen by the streaky-to-spotty transition between 2- and 4-hours indicating island formation [8]. This transition appears at all nitridation temperatures in the range of 3 to 4 hours. One possible explanation for this surface evolution is the saturation of the GaN film accompanied by GaN decomposition. Once the GaN film is established, decomposition produces chemi-desorbed gallium atoms [8] which are free to diffuse across the surface. Therefore, impinging highly reactive nitrogen species can react with stray Ga atoms forming islands of GaN rather than exchange with the previously readily available oxygen of the oxide surface, resulting in rougher surfaces and spotty RHEED patterns.

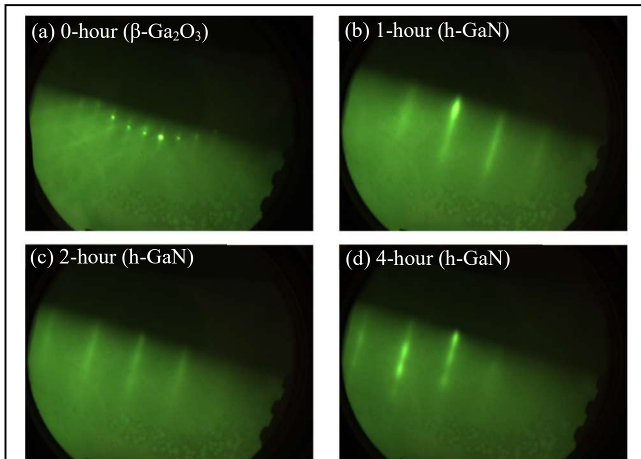

Fig. 1. RHEED pattern transformation from β-Ga_2O_3 to wurtzite GaN at 700˚C. Prolonged exposure to nitrogen plasma after establishing the GaN film results in island formation (streaky-to-spotty transition in (d)).

In contrast to documented GaN phase transformation on (100) β-Ga_2O_3, no cubic phase transition was detected [10]. Difference in phase progression may be attributed to the use of an RF plasma for the source of nitrogen rather than an ammonia source, or the decreased lattice mismatch for wurtzite GaN on (-201) β-Ga_2O_3 compared to (100) [5,10,14,15].

Holding the nitrogen plasma source conditions constant at 1.3 sccm and 400 W, the surface roughness was measured by AFM on an Asylum Cypher (Table 1) across the temperature range 600-725˚C after 210min of nitridation. The roughness is roughly linearly (Fig. 2) corelated with nitridation temperature. As the substrate temperature approaches that of GaN decomposition, the roughness increases. This supports the notion discussed previously that GaN decomposition is likely one contributing factor to surface roughness of nitridated β-Ga_2O_3.

The FWHM of the rocking curves about the (0002) GaN reflection are listed in Table 1 and 2. The FWHM of 644 arcsec represents substantial progress using such methods of buffer layer growth through nitridation [10]. Characterization of UID GaN grown utilizing these buffer layers is expanded in our sister paper [F.P. Kelly, Development of GaN-on-Ga_2O_3 Heterostructures for Vertical Power Devices, Paper #7.4].

TABLE 1: TEMPERATURE DEPENDENCE OF NITRIDATED β-Ga_2O_3

Temperature [˚C]	Roughness [nm]	FWHM (0002) [arcsec]	Thickness [nm]
600	0.454	786	4.40
650	0.544	681	4.72
675	0.658	773	5.21
700	0.761	802	5.75
725	0.864	775	2.87

Film thickness was extracted from X-Ray reflectivity measurements and plotted against nitridation temperature in Figure 2. Temperatures greater than 700˚C result in a reduced thickness, attributed to entering a regime of rapid GaN decomposition which competes with the diffusion front propagating into the oxide. Below 700˚C, the film thickness decreases, the temperature dependence of the diffusion coefficient becomes evident, supporting the theory that nitrogen diffusion fuels the phase transformation.

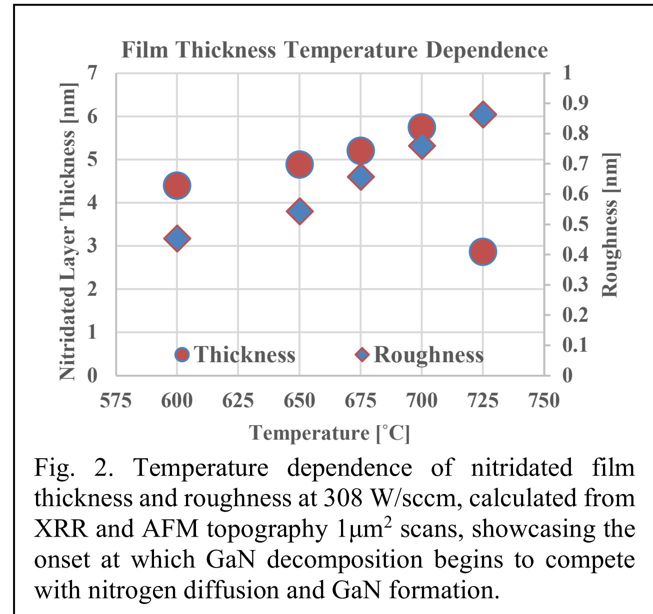

Fig. 2. Temperature dependence of nitridated film thickness and roughness at 308 W/sccm, calculated from XRR and AFM topography 1μm^2 scans, showcasing the onset at which GaN decomposition begins to compete with nitrogen diffusion and GaN formation.

To determine the effects of plasma composition, power and flow rate, plasma power-density was varied between 100-470 W/sccm. Film thickness and roughness were calculated as described previously and are plotted against plasma power-density at two nitridation temperatures of 650˚C and 700˚C in Figure 3. The surface roughness is increased at 700˚C for equivalent power densities, keeping with the trend seen in Figure 2 in the regime prior to significant GaN decomposition. In all cases, roughness decreases at high

power densities, achieving the lowest value of 0.31 nm at 470 W/sccm and 650˚C.

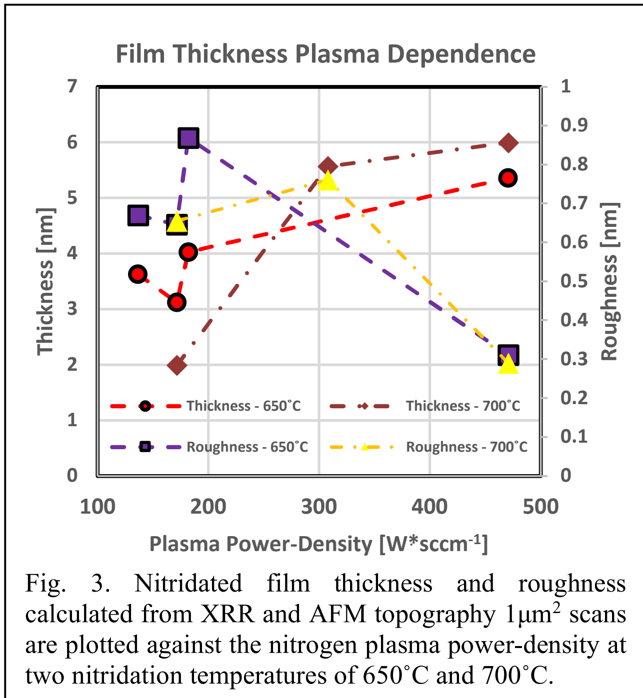

Fig. 3. Nitridated film thickness and roughness calculated from XRR and AFM topography 1µm^2 scans are plotted against the nitrogen plasma power-density at two nitridation temperatures of 650˚C and 700˚C.

High power densities also resulted in thicker nitridated films. Analyzing the plasma spectra at various power densities reveals increased emission intensity from atomic nitrogen at high power density, and lower emission intensity from molecular nitrogen species. In other words, the ratio of atomic to molecular nitrogen at the sample surface increases at high power density. This suggests that the highly energetic atomic nitrogen drive the phase transformation, resulting in thicker films.

TABLE 2: POWER-DENSITY DEPENDENCE OF NITRIDATED β-Ga_2O_3

Power Density [W/sccm]	Roughness [nm]	FWHM (0002) [arcsec]	Thickness [nm]
650 ˚C			
136*	0.669	691	3.63
171*	0.645	665	3.12
181**	0.868	691	4.03
470**	0.311	713	5.36
700 ˚C			
171*	0.655	412	1.99
308**	0.761	802	5.57
470**	0.347	644	5.995
*300 W plasma power **400 W plasma power			

It should be noted that to stay within safe operating conditions, power density was increased by reducing the flow rate from 2.2sccm to 0.85sccm at 400W, therefore the overall flux of nitrogen is reduced at higher power density. Strictly increasing the plasma power may result in different trends.

UID GaN epitaxy on the nitridated surface showed reduced defect density with thicker nitridated layers. UID GaN on Ga_2O_3, nitridated at 700˚C and 470 W/sccm, has an X-Ray rocking curve (XRC) FWHM of 190 arcsec, representing substantial progress for GaN-on-Ga_2O_3 as a material platform for power device applications.

CONCLUSION

Nitrogen RF-plasma was used to nitridate β-Ga_2O_3 to GaN with varying substrate temperature, duration, and plasma power density. Nitridated layers were characterized via AFM, XRD, RHEED, and XRR. AFM measurement revealed that surface roughness increases linearly with substrate temperature in this range and is reduced at high power densities. GaN decomposition at high temperatures may contribute to island formation and increased roughness. Film thickness was extracted from reflectivity oscillations and supports the hypothesis that the progression of nitridation is dependent on the competing processes of nitrogen diffusion and GaN decomposition. UID GaN on nitridated Ga_2O_3 achieved an XRC FWHM of 190 arcsec, proving the potential of GaN-on-Ga_2O_3 as a wide-bandgap power device platform.

ACKNOWLEDGEMENTS

Data was collected at the Frederick Seitz Materials Research Laboratory. This work was supported by the Office of Naval Research Award N00014-21-1-2544 (PM: Lynn Petersen).

REFERENCES

[1] S. J. Pearton et al. Applied Physics Review 5, 011301 2018

[2] Chenlu Wang et al. Journal of Physics D: Applied Physics, 54 243001 2021

[3] Varley et al. Physical Review B, 85 081109(R) 2012

[4] Zhang K H L, et al. Journal of Physics: Condensed Matter, 28 383002 2016

[5] M.M. Muhammed et al. Scientific Reports, 6 29747 2016

[6] Weijiang Li et al. Journal of Applied Physics, 127 015302 2020

[7] N. Zhu et al. Applied Surface Science, 586 152831 2022

[8] S. Fernandez-Garrido et al. Journal of Applied Physics, 104 033541 2008

[9] S. Besendorfer et al. Journal of Applied Physics, 127 015701 2020

DISTRIBUTION STATEMENT A. Approved for public release; distribution unlimited.

[10] S. Ohira et al. Physica Status Solidi C, 4 7 2007

[11] T. J. Anderson et al. IEEE Transactions on Semiconductor Manufacturing, 29 4 2016.

[12] P. Sarker et al., IEEE Journal of the Electron Devices Society, 9 2021

[13] H. Kim, Electronics Letters, 44 17 2008

[14] D. Li et al. Journal of Crystal Growth, 478 201 2017

[15] Encarnación G. Víllora et al. Applied Physics Letters, 90 234102 2007

Acronyms

PAMBE – PLASMA-ASSISTED MOLECULAR BEAM EPITAXY
AFM – ATOMIC FORCE MICROSCOPY
XRD – X-RAY DIFFRACTION
XRR – X-RAY REFLECTIVITY
MOCVD – METAL ORGANIC CHEMICAL VAPOR DEPOSITION
MOVPE – METAL ORGANIC VAPOR PHASE EPITAXY
RHEED – REFLECTION HIGH ENERGY ELECTRON DIFFRACTION
SCCM – STANDARD CUBIC CENTIMETERS PER MINUTE
UID – UNINTENTIONALLY DOPED
RF – RADIO FREQUENCY
XRC – X-RAY ROCKING CURVE

DISTRIBUTION STATEMENT A. Approved for public release; distribution unlimited.